ORIGINAL CONTRIBUTION

SLE$_3$S-water system: a linear rheological characterisation

Rosalia Ferraro[1,2] · **Sergio Caserta**[1,2]

Abstract

Surfactant-water mixtures display a complex rheological behaviour, with changes in parameters such as viscosity and moduli of several orders of magnitude as a consequence of phase changes, depending on their concentration and temperature: this criticism heavily affects different industrial processes. In our work, linear rheological behaviour of aqueous mixtures of a commercial anionic surfactant, sodium lauryl ether sulphate, is investigated in a range of temperature (30–60 °C) and surfactant concentration (20–72%wt) of technological relevance. Four phases with different texture are identified by polarised light microscopy: micellar, hexagonal, cubic and lamellar, all showing a shear-thinning behaviour. Rheological parameters of cubic phase show a net jump in a relatively narrow temperature range, suggesting a temperature-induced phase change. The systematic analysis of the rheological behaviour of this widely used surfactant system, reported here for the first time, can be of fundamental support for many industrial applications.

Keywords Sodium lauryl ether sulphate · Anionic surfactants · Temperature effect · Cubic phase · Phase changes

Introduction

Surfactants are amphiphilic molecules characterised by a hydrophobic tail and a hydrophilic head, fundamental for an extremely wide range of applications, such as home- and beauty-care, everyday use goods (Baruah et al. 2015; Hargreaves 2007; Yang 2002), food (Drakontis and Amin 2020) and pharmaceutical industry, including development of drug delivery systems, such as liposomes (Garti et al. 2012; Guo et al. 2010).

Highlights

●Distinct textures of surfactant-water system are identified by using polarised light microscopy.
●Rheological properties of SLE$_3$S/H$_2$O system are investigated in a range of temperature (30–60 °C) of technological relevance.
●Cubic liquid crystalline phase shows temperature variations of several orders of magnitude in viscosity and moduli.
●Rheology represents a powerful tool to characterise different phases in surfactant-water systems, such as polarised light microscopy, and can be used to provide a systematic phase diagram.

✉ Sergio Caserta
  sergio.caserta@unina.it

1 Dipartimento di Ingegneria Chimica, dei Materiali e della Produzione Industriale, Università degli Studi di Napoli Federico II, 80125 Napoli, NA, Italy

2 CEINGE Advanced Biotechnologies, 80145 Naples, Italy

Due to their complex molecular structure, as the surfactant concentration in a water solution increases, the system undergoes a series of phase changes. In detail, as soon as surfactant concentration overcomes a critical value, known as critical micellar concentration (typically order of 10^{-2} mM) (Hait and Moulik 2001; Mahmood and Al-Koofee 2013; Ohlendorf et al. 1986), surfactant molecules self-assemble and form micelles (spherical, rod-like or wormlike) (Davies et al. 2006; Yang 2002). Different types of micelles correspond to different morphological structures and specific rheological properties, even in the case of highly diluted micellar solutions that can be weakly viscoelastic in the case of wormlike structures (Acharya and Kunieda 2006; Imae et al. 1985; Panmai et al. 1999; Trickett and Eastoe 2008). As surfactant concentration grows (typically above 20%wt), different grades of order in the amphiphilic molecules are realised. In these conditions, molecules organise themselves in hexagonal, cubic or lamellar crystalline liquid structures (Fontell 1990) which lead to a complex physical-chemical behaviour (Richtering 2001).

Concerning rheology, concentrated surfactant-water solutions, usually defined as surfactant pastes, show a gel-like behaviour. In high concentration range, heavily different rheological behaviours are observed, with non-monotonic changes in viscosity and moduli of several orders of magnitude. These changes not only depend on concentration, but also on temperature

(Acharya and Kunieda 2006, Cappelaere et al. 1994, Castaldo et al. 2019, Davies et al. 2006, Ketner and Raghavan , Kumaran et al. 2001, Li et al. 2016, Poulos et al. 2017). These two key parameters also affect other physical properties, related to the molecular order induced in the fluid.

Previous works (Johnston et al. 2015; Panoukidou et al. 2019; Rekvig et al. 2003; Skartlien et al. 2012) investigated phase diagram of water-surfactant systems, including predictions on rheological behaviour, only in silico, due to problems associated to experimental characterisation. Consequently, a detailed understanding of rheological behaviour of surfactants at different water content and, in particular, at temperatures higher than room temperature is crucial (Baruah et al. 2016, Pathak and Ojha , Kekicheff et al. 1989, Luo et al. 2012).

The main goal of this work is to fill this gap in the knowledge, providing a systematic rheological characterisation, not available in the literature, of one of the most used anionic surfactants: sodium lauryl ether sulphate (SLE_3S). SLE_3S is one of the main components in shampoos, detergents, toothpastes and creams, used for its emulsifying and foaming properties and for its reduced production costs. Understanding the physics of these systems plays a key role in industrial processing, which also has an important impact on production efficiency.

In this paper, in order to identify different textures of the water-based mixture, related to the SLE_3S concentration, and to obtain macroscopic qualitative information on sample structure, optical anisotropy properties of each phase are observed by using polarised light microscopy (PLM). Then, the systematic rheological characterisation of each texture is performed at different temperatures, in the range 30–60 °C, in order to determine changes in shear viscosities and moduli, a key issue in ruling formulation functionality (Capaccio et al. 2020; Dehghan et al. 2015; Jiang et al. 2009). A special attention is paid to the cubic phase which exists only in a narrow concentration range and, for this reason, is not easy to identify. Consequently, cubic phase is often poorly characterised (Lavergne et al. 2011), despite being related to most of the difficulties faced in industrial processes, due to a dramatic increment in rheological parameters (viscosity and moduli) respect to the neighbouring phases.

The approach here proposed, focused on the range of concentration and temperature of industrial relevance, can be used as a simple and effective way to obtain a detailed phase map of a multicomponent mixtures exhibiting complex phase behaviour.

Materials and methods

Chemical structure

SLE_3S is a sodium salt produced through the ethoxylation of the sodium lauryl sulphate (SLS), characterised by a similar structure with three extra ether groups (Cserháti et al. 2002). The hydrophilic head of SLE_3S includes three ether groups and a SO_3^- group, balanced by a Na^+ counterion. According to typical behaviour of surfactant systems, depending on concentration in water, SLE_3S rearrange in different morphologies, corresponding to different phases. In detail, at room temperature (25 °C), phase changes are defined in the following concentration ranges: micellar (referred as L_1) in the range 0.024–28%wt, hexagonal (H) 31–56%wt, cubic (V_1) ~ 58–62%wt and lamellar (L_α) 62–72%wt (Li et al. 2016).

Sample preparation

SLE_3S solution is obtained from Procter and Gamble in the form of a high concentrated paste (72% weight fraction surfactant in water, as determined by vacuum drying). Samples (~5 g each) at different concentration (20, 35, 50 and 60%wt) are prepared using distilled water to dilute the surfactant raw paste using an analytical balance (sensitivity 10^{-4} g). Concentrations are selected to fall within the L_1, H, V_1 and L_α domains, respectively. The samples are carefully mixed using a spatula and centrifuged (4000 rpm for 40 min) to degas them. Centrifugation step is repeated more than one time due to the high viscous samples, until a bubble-free sample is obtained. Samples are then stored at room temperature overnight to guarantee the equilibrium and the homogeneity. Preliminary visual inspection through cross-polarisers is used to check phase uniformity in the samples.

Optical setup

PLM is used to check texture of SLE_3S samples and to identify the correlation between the concentration and the corresponding phase. Optical setup is based on an inverted microscope (Zeiss Axiovert 200, 20× objective) equipped with a high-sensitivity CCD video camera (Hamamatsu Orca AG) and a motorised stage (Marzhauser), controlled by an in-house-built software, for automated mosaic scanning of large samples (Ferraro et al. 2022).

A tiny amount of surfactant at different concentration is squeezed between a glass microscope slide and a coverslip. Sample thickness is set at 130 µm by inserting a double-side adhesive tape as a spacer between the two glass surfaces. Sample thickness is verified by measuring the focus position, by means of the microscope focus encoder, of top and bottom glass surfaces confining the surfactant paste. Two crossed polarised filters are placed before and after the sample along the optical path. 3×3 mosaic images are acquired at room temperature and sticked using commercial image analysis software (Image-Pro Plus). Sample birefringence, related to the ordered texture in SLE_3S morphology, allows

to identify different phases by simple visual comparison (see Fig. 1). Further detail on the methodology, including a cartoon of experimental setup here described, is reported in a previous work (see Fig. 1 D in Capaccio et al. 2020).

Rheological setup

Rheological measurements are performed at different temperatures (30, 40, 50 and 60 °C) using a stress-controlled rheometer (Anton Paar Physica MCR 301 Instruments) (Tomaiuolo et al. 2016) equipped with a double gap measuring system (C-DG26.7-20/T200/S and DG26.7/TI) for sample characterised by a low viscosity (20%wt) and a cone-plate measuring system (CP25-1/S-SN72510) for sample characterised by a high viscosity (35, 50, 60 and 72%wt). Temperature is controlled by a Peltier cooler/heater connected to a circulating water bath (Lauda) and let to equilibrate at the measuring value for 3 min before each test.

Pre-shear is run to homogenise sample structure after loading, imposing a constant shear rate ($\dot{\gamma}$) of 200 1/s for 1 min. For H, V_1 and L_α, flow curves are run varying $\dot{\gamma}$ in the range 0.01–200 1/s (40 data points, sampling time 15 s). Measurements are repeated varying $\dot{\gamma}$ from 200 to 0.01 1/s. For L_1, flow curves are run varying $\dot{\gamma}$, from 10 to 200 1/s, and vice versa, to minimise noise related to rheometer sensitivity at low torque. No significant differences (hysteresis) are observed comparing the $\dot{\gamma}$ rising and decreasing tests, for simplicity only 0.01–200 1/s data are reported in the results.

To identify the linear viscoelasticity range, strain sweep experiments are performed. Storage and loss moduli (G' and G'', respectively) are measured at fixed angular frequency ($\omega = 5$ rad/s) varying the strain in the range 0.01–200. For all the tests, linear viscoelasticity is verified in the range of amplitude 0.01–1 s. Frequency sweep is investigated at strain 0.1 varying frequency in the range 100–0.1 rad/s, measuring 16 data points, except for L_1 where the range is 10–0.1 rad/s.

The entire characterisation required about 45 min for each T. To limit water evaporation and phase transitions due to concentration changes during the rheological measurements, sample is reloaded for each T measured.

Parallel plate rheo-optical apparatus

In order to verify the influence of shear flow on phase changes, some preliminary rheo-optical tests are run at room temperature. In particular, we focused this analysis on the SLE_3S concentration that showed the most complex phase behaviour (60%wt). A simple shear flow is generated by using a parallel plate rheo-optical apparatus, widely described in previous works (Caserta et al. 2004; Caserta et al. 2006; Pommella et al. 2012). Briefly, one of the two optical glass plates is translated with respect to the other by a computer controlled motorised stage (Ludl). The flow cell containing the sample is under the field of view of an optical microscope (Zeiss Axioscope). Also in this case, two polarised filters, placed on top and on bottom of the two glass plates, are carefully crossed and fixed to visualise sample birefringence. Sample can be observed by a high-speed video camera (Hamamatsu C11440-36u) along the velocity gradient direction. Image acquisition rate is fixed to 1 image/s.

Texture evolution is investigated in a range of $\dot{\gamma}$ similar to the one used in rheological measurements (0.01–200 1/s). In this case, $\dot{\gamma}$ is given by the ratio between the speed of the moving plate and the gap between plates, fixed to 130 μm, in analogy with the static image acquisition (see "Optical setup" section). To quantify the texture evolution, light intensity is calculated by measuring the average grey level (I), normalised respect to image intensity at rest (I_0) as function of time, at different $\dot{\gamma}$.

Data, reported in supplementary (see Fig. S1), do not show texture variations comparable with the one induced by temperature and concentration changes. For this reason,
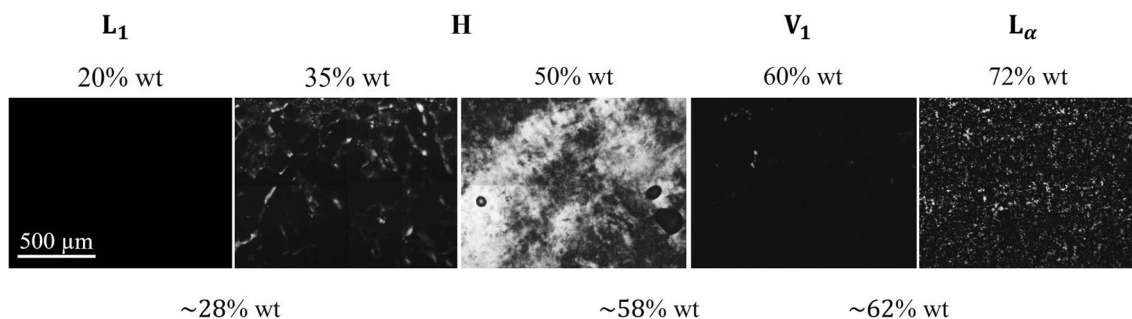

Fig. 1 Optical experiments: five different concentrations of SLE_3S are compared, at room temperature, in order to visualise four distinct phases, i.e., micellar (L_1), hexagonal (H), cubic (V_1) and lamellar (L_α). At the bottom of the panel, the critical concentration values denoting the transition from one phase to another are also given (~28% wt from micellar to hexagonal, ~58% wt from hexagonal to cubic and ~62% wt from cubic to lamellar)

we considered as negligible the influence of flow on sample transitions, respect to variations induced by temperature and concentration, in the range of values here investigated.

Statistical data analysis

All rheological characterisations are performed at least two times on different samples prepared independently, repeating the dilution from the same 72% batch. Data reported in the charts are expressed as mean ± standard error of the mean (SEM).

Results

The scope of this work is to provide a systematic rheological characterisation of phases exhibited in the SLE$_3$S/H$_2$O system, not still available in the literature. To this aim, a preliminary sample characterisation is run at room temperature by PLM in order to distinguish different phases, related to the concentration system. Each of the so identified textures is than object of a detailed rheological characterisation in a range of temperature 30–60 °C. Measuring the influence of concentration and temperature on rheological properties represents an innovative way to support industries and their processes. In the following section, experimental results are presented.

Phase characterisation

In Fig. 1, mosaics scanning images of the sample at different concentrations and, consequently, representative of different phases are reported. In fact, comparison of optical properties and image brightness provides information on the sample phase here compared (L$_1$, H, V$_1$ and L$_\alpha$).

L$_\alpha$ is clearly identified by typical Maltese cross patterns, visible in the 72%wt sample. By reducing the concentration, sample at 60%wt appears almost completely black, with the sole exception of some isolated light spots, in agreement with an isotropic cubic phase, that appear already qualitatively very stiff. This phase is present in a very narrow concentration range of approximatively 58–62%wt. Further reducing SLE$_3$S concentration, H is expected to be birefringent, as the cloudy samples corresponding to 50%wt. Sample at 35%wt denotes the transition from hexagonal to micellar phase: in this case, indeed, the texture shows a not uniform brightness, with bright domains separated by dark regions, suggesting a phase equilibrium between H and L$_1$, as reported in most phase diagrams, differently from L$_1$ which appears completely black.

Rheological characterisation

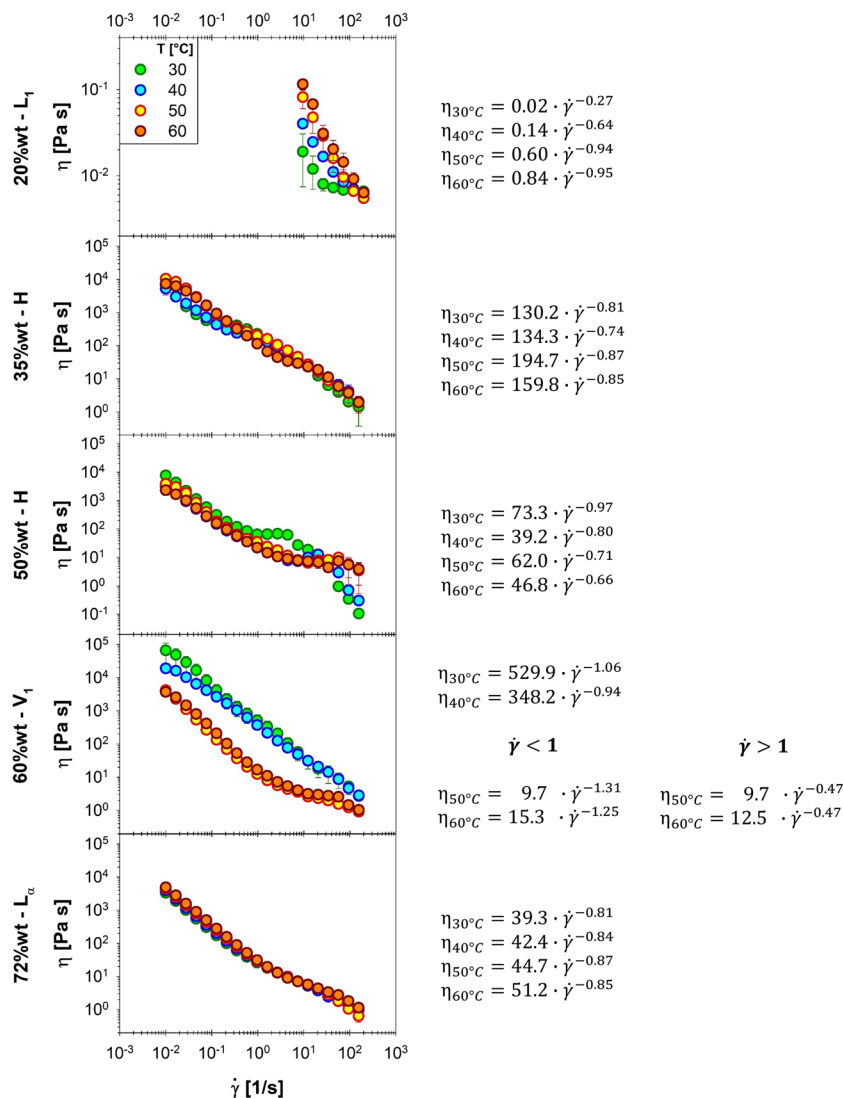In this section, a detailed rheological characterisation of the system under investigation is reported. Both flow and frequency test are run using the constant stress rheometer equipped with the geometry and protocol described above (see "Rheological setup" section).

Flow curve

In Fig. 2, viscosity (η) measurements as a function of $\dot{\gamma}$ are shown for the five concentrations here in exam (20, 35, 50, 60 and 72%wt), corresponding to four different phases (L$_1$, H, V$_1$ and L$_\alpha$), for four different temperatures (30, 40, 50 and 60 °C). In agreement with previous measurements at room temperature reported in the literature (Castaldo et al. 2019), all the samples show a typical shear thinning behaviour, with a viscosity decrement of ~4 orders of magnitudes in the range of shear rate here investigated. In particular, viscosity of hexagonal (H, 35 and 50%wt) and lamellar (L$_\alpha$, 72%wt) samples decreases as function of $\dot{\gamma}$ from 10^3 to 1 Pas, with limited differences by varying T in the range investigated. In the case of micellar phase (L$_1$, 20%wt) and cubic phase (V$_1$, 60%wt), a stronger dependency of η from T is observed. For L$_1$, at fixed shear rate (e.g,. $\dot{\gamma} \sim 10$ 1/s), η increases of one order of magnitude, from 0.02 to 0.12 Pas, increasing temperature from 30 to 60 °C. This unusual increase in viscosity with temperature probably depends on increments in the contour length of micelles, in fact, at high temperatures micelles are known to grow into longer and flexible cylinders (Kalur et al. 2005). In the case of V$_1$, at low T values (30 and 40 °C), η thins from 10^4 to 10^1 Pas with $\dot{\gamma}$. In these conditions, V$_1$ is more viscous respect to both H and L$_\alpha$ phases. On the contrary, in high T range (50–60 °C), η of cubic phase is considerably reduced. Considering data at fixed value of $\dot{\gamma}$ (e.g. 1 1/s), η of V$_1$ phase is about $4 \cdot 10^2$ Pas at 30 and 40 °C, while is about $1.5 \cdot 10^1$ Pas at 50 and 60 °C. Such a stronger decrement of η with T suggests a phase transition (Baruah et al. 2015).

To better investigate how T affects rheological behaviour of each phase, flow curves are fitted with a power-law viscosity model ($\eta = k \cdot \dot{\gamma}^{n-1}$), where k is the consistency factor and n is the flow exponent. As shown in the legends reported in Fig. 2, $n < 1$ for all conditions investigated, in agreement with a typical shear thinning fluid, corresponding to a linear trend in the logarithmic diagrams. Data lies on a single line in the entire range of observation ($10^{-2} < \dot{\gamma} < 10^2$ 1/s), for surfactant concentration 20, 35 and 72%wt. In the case of L$_1$ sample, a variation with T is observed in both fitting parameters: in particular, k increases (from 0.02 to 0.84 Pas), while n decreases with temperature (from −0.27 to −0.95), consequently viscosity radically increase heating from 30 to 60 °C. Similar increment of about 1 order of magnitude in viscosity of cationic and anionic micellar solution as function of temperature (Kalur et al. 2005) or pH (Zhang et al. 2013) is previously observed and attributed to the growth of wormlike micelles. Marginal fluctuations for the sample

Fig. 2 Influence of shear rate and temperature (30 °C—green, 40 °C—blue, 50 °C—yellow, 60 °C—orange) on viscosity for five concentrations of SLE$_3$S (20, 35, 50, 60 and 72%wt). Flow curves are fitted with a power-law viscosity model (fitting are reported on the right), in order to evaluate flow parameters (n and k) for each concentration at different temperatures. In detail, V$_1$ flow curves at 50 and 60 °C are split in two sections ($\dot{\gamma} < 1$ 1/s and $\dot{\gamma} > 1$ 1/s) to better investigate the effect of temperature on viscosity

$\eta_{30°C} = 0.02 \cdot \dot{\gamma}^{-0.27}$
$\eta_{40°C} = 0.14 \cdot \dot{\gamma}^{-0.64}$
$\eta_{50°C} = 0.60 \cdot \dot{\gamma}^{-0.94}$
$\eta_{60°C} = 0.84 \cdot \dot{\gamma}^{-0.95}$

$\eta_{30°C} = 130.2 \cdot \dot{\gamma}^{-0.81}$
$\eta_{40°C} = 134.3 \cdot \dot{\gamma}^{-0.74}$
$\eta_{50°C} = 194.7 \cdot \dot{\gamma}^{-0.87}$
$\eta_{60°C} = 159.8 \cdot \dot{\gamma}^{-0.85}$

$\eta_{30°C} = 73.3 \cdot \dot{\gamma}^{-0.97}$
$\eta_{40°C} = 39.2 \cdot \dot{\gamma}^{-0.80}$
$\eta_{50°C} = 62.0 \cdot \dot{\gamma}^{-0.71}$
$\eta_{60°C} = 46.8 \cdot \dot{\gamma}^{-0.66}$

$\eta_{30°C} = 529.9 \cdot \dot{\gamma}^{-1.06}$
$\eta_{40°C} = 348.2 \cdot \dot{\gamma}^{-0.94}$

$\dot{\gamma} < 1$	$\dot{\gamma} > 1$
$\eta_{50°C} = 9.7 \cdot \dot{\gamma}^{-1.31}$	$\eta_{50°C} = 9.7 \cdot \dot{\gamma}^{-0.47}$
$\eta_{60°C} = 15.3 \cdot \dot{\gamma}^{-1.25}$	$\eta_{60°C} = 12.5 \cdot \dot{\gamma}^{-0.47}$

$\eta_{30°C} = 39.3 \cdot \dot{\gamma}^{-0.81}$
$\eta_{40°C} = 42.4 \cdot \dot{\gamma}^{-0.84}$
$\eta_{50°C} = 44.7 \cdot \dot{\gamma}^{-0.87}$
$\eta_{60°C} = 51.2 \cdot \dot{\gamma}^{-0.85}$

at 50%wt, also in the H phase region, can be observed: a variation with T is observed in both fitting parameters, in particular n increases from −0.97 to −0.66. In the case of V$_1$ phase sample (60%wt), η at high T shows a clear discontinuity at $\dot{\gamma} \cong 1$ 1/s. For this reason, flow curves at 50 and 60 °C are split in two sections ($\dot{\gamma} < 1$ 1/s and $\dot{\gamma} > 1$ 1/s), obtaining two independent values of power law fittings parameters, also reported in figure legend. From the above observation, we can state that flow parameters, referred as k and n, are a step function of T only for V$_1$ phase, while they show minor changes for other phases, in the same range of T investigated. This observation is in agreement with the expected phase transition in this concentration and temperature range.

As regards the cubic phase, in order to better investigate the T effect on these rheological aspects, η is measured at additional temperatures (20, 45 and 48 °C). In Fig. 3, η data (y-axis) are plotted as a function of $\dot{\gamma}$ (x-axis) and T (z-axis). As shown in the 3D plot, η show limited changes in the entire range 20–45 °C. At 48 °C, η begins to significantly
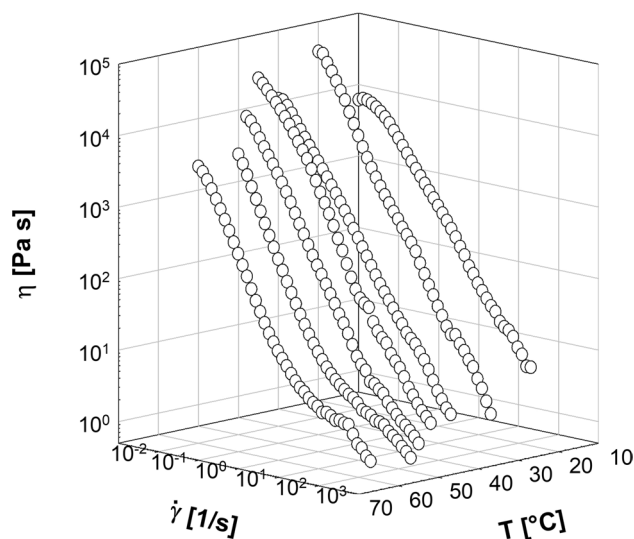

Fig. 3 Influence of shear rate (x-axis) and temperature (z-axis) in the range 30–60 °C on viscosity (y-axis) of SLE$_3$S cubic phase (60%wt)

decrease (~4× times) and then collapse considerably of 1 order of magnitude at 50 and 60 °C.

To estimate η-T dependency, a classical Arrhenius-like equation (Baruah et al. 2016) is used ($\eta(T) = Ae^{E_a/RT}$), where R (J/mol K) is the universal gas constant and E_a (J/mol) is the activation energy. As shown in Fig. 4, E_a can be estimated from the linear slope (dotted line) obtained by plotting k values, reported in Fig. 2 (i.e., $k = \eta|_{\dot\gamma=1}$ for H, V$_1$ and L$_\alpha$ and $\eta|_{\dot\gamma=10}$ for L$_1$), as function of $1/T$. The low activation energy value indicates the presence of stable structures (Baruah et al. 2015) and of limited influence of T on η. As shown, H and L$_\alpha$ phases are characterised by low values of E_a, ~0, 7.6 and ~0 kJ/mol, respectively. On the contrary, due to unusual increase in viscosity with temperature, L$_1$ (20%wt) is characterised by a negative value of E_a (~−5.1•10^4 kJ/mol). As regards V$_1$ (60%wt), three different regions can be distinguished: two regions characterised by low values of E_a (9.0 and 13.0 kJ/mol, for low and high values of $1/T$, respectively), where η marginally changes in the range of T investigated; in the intermediate region, an higher value of E_a, ~4.6•10^2 kJ/mol is measured, indicating the existence of a phase transition in the temperature range 45–50 °C.

Oscillatory tests

Performing frequency sweep tests, G' and G'' are investigated as function of ω. Measurements at 30 and 60 °C are reported in Fig. 5, while frequency sweep tests at 40 and 50 °C are reported in Supplementary Materials for brevity. In the temperature range examined, G' (triangle up) is always higher respect to G'' (triangle down) with an almost parallel trend, suggesting a weak-gel-like behaviour (Trappe and Weitz 2000) of surfactant pastes. Both moduli slightly increase with T for L$_1$, H and L$_\alpha$, while V$_1$ shows a significant reduction of G' and G'' going from 30 to 60 °C, confirming phase changes previously observed.

To better investigate moduli changes, the ratio between G'' and G', i.e., tan(δ), is evaluated and plotted as function of ω for all experimental conditions (Fig. 6 data at 30 and 60 °C, Supplementary Materials data at 40 and 50 °C). As shown, heating poorly affects tan(δ) for H and L$_\alpha$, while for V$_1$ tan(δ) increases significantly with T: in detail, at 60 °C, the ratio is about 2.8× higher respect to the value at 30 °C. Indeed, for cubic samples at high temperature the difference between the two moduli reduces, although G'' remains lower than G'.
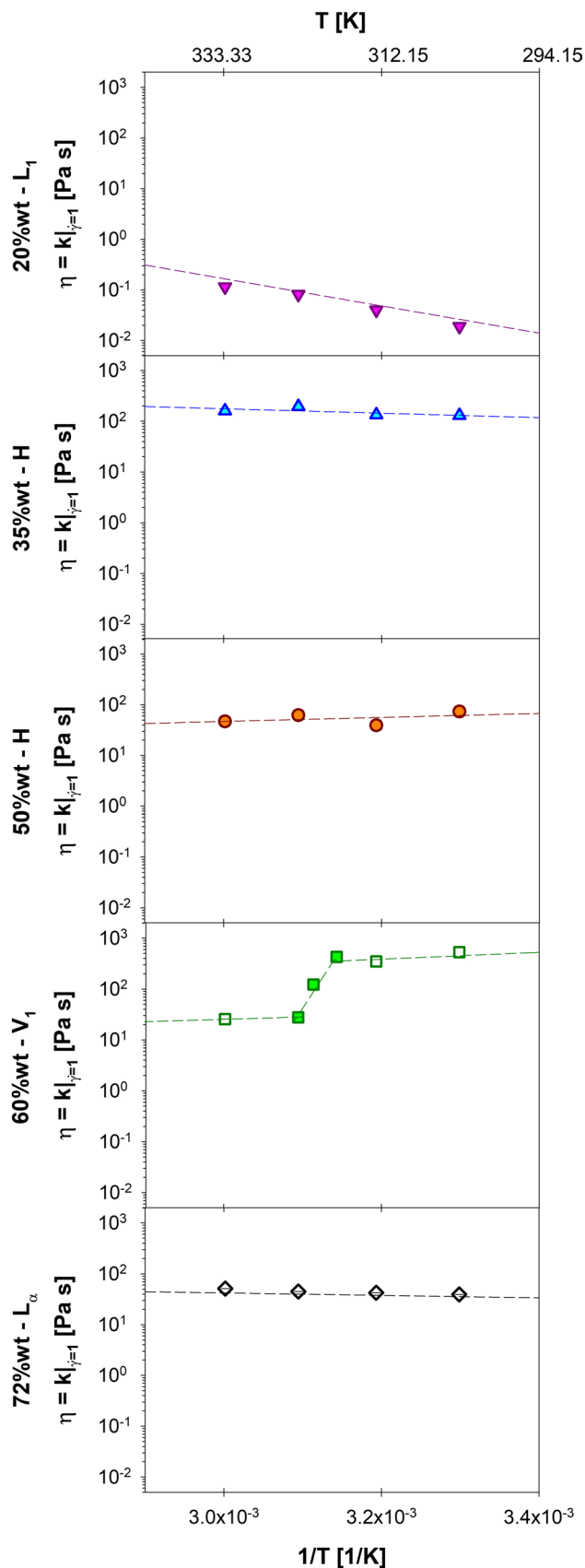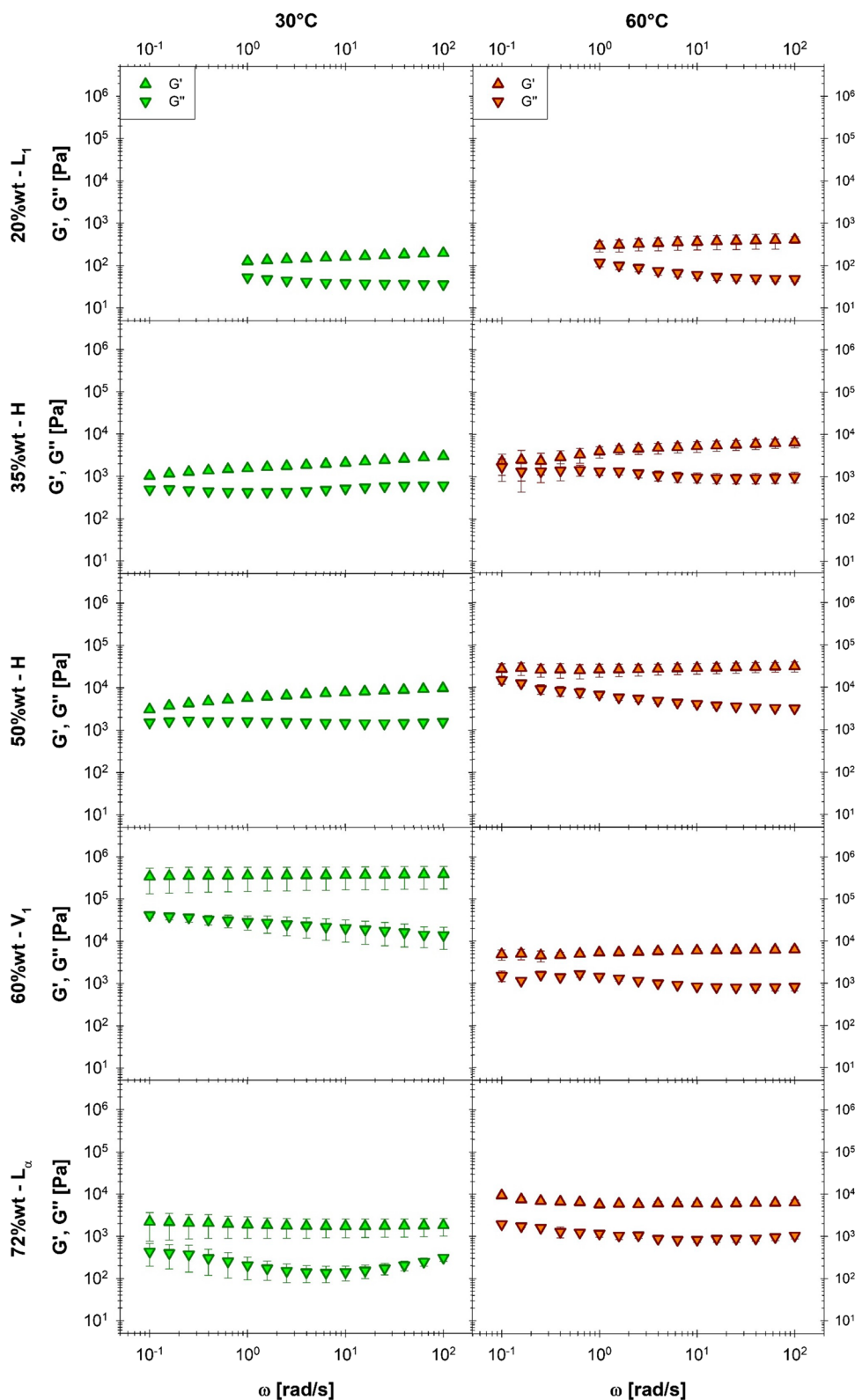
Fig. 5 For each SLE$_3$S concentration investigated (20, 35, 50, 60 and 72%wt), elastic (G', Pa) and viscous (G'', Pa) moduli are reported as function of angular frequency (ω, rad/s), triangle up and down, respectively. Experimental data are reported at two different temperature, 30 and 60 °C (green symbols on the left and orange symbols on the right, respectively). In Supplementary Materials, same measurements are also reported for 40 and 50 °C

Temperature effect

Measurements reported above are here used to identify rheological properties of different phases and, consequently, different surfactant concentration in water as function of a temperature range (30–60 °C) of technological relevance, in order to provide a deep characterisation of SLE$_3$S-water system. In Fig. 7, η and complex viscosity (η^*) data are plotted,

Fig. 6 tan(δ), calculated as the ratio between G'' and G', is reported as ▶ function of angular frequency (ω, rad/s), at 30 and 60 °C (green and orange circles, respectively) for each SLE$_3$S concentration investigated (20, 35, 50, 60 and 72%wt). In Supplementary Materials, same measurements are also reported for 40 and 50 °C

at fixed $\dot{\gamma}$ (=1 1/s) and at fixed ω (=1 rad/s), against the whole range of T for all SLE$_3$S concentration investigated. In L$_1$, H and L$_\alpha$ region, η shows a limited change as function of T, while η jumps is clearly visible in V$_1$ data series, as previously described. In detail, SLE$_3$S at 60%wt, at $\dot{\gamma}$ = 1 1/s and T = 30 °C, has a η ~3.5× and ~20× higher than H and L$_\alpha$ phases, respectively, while at high T, e.g., 60 °C, the same concentration range shows a reduced η respect to the other phases (~0.25× and ~0.54× compared to H and L$_\alpha$, respectively).

In Fig. 7, complex viscosity η^* is compared to η (left and right panels). The general trend of data is the same, with limited changes in both viscosities with T for all the phases except V$_1$. However, Cox-Mertz superposition rule is not valid, as evident observing values of η^* are systematically more than one order of magnitude higher respect to η. It is worth noticing temperature dependency of η^* is stronger compared to η.

The same behaviour can be also observed plotting G', G'' and complex modulus (G^*) against T, parametric in SLE$_3$S concentrations (Fig. 8). Also in this case, significant changes in rheological response of surfactant pastes are observed. In particular, moduli of V$_1$ are significantly higher respect to L$_1$, H and L$_\alpha$ phases at low T, but dramatically reduce increasing this parameter: in detail, G' decreases from 3.6•10^5 to 4.2•10^3 Pa, G'' from 2.7•10^4 to 4.7•10^3 Pa and G^* value from 2.9•10^5 to 5.4•10^3 Pa. In the same temperature range, moduli of other phases show only minor fluctuations. It is worth noting the phase change observed for V$_1$ phase systems as function of T appears to be in the range 40–50 °C, observing shear viscosity jump, while oscillatory tests seem to suggest a slightly lower value of the T transition, that is measurable in the range 30–40 °C.

Discussion and conclusions

Surfactants, due to their complex molecular structure, undergo a series of phase changes, depending on their concentration and temperature, affecting different parameters. In particular, a detailed characterisation of flow behaviour is needed for an adequate design of industrial processing. Despite this, such a characterisation is not available in the literature, neither for systems of common industrial use, such as sodium lauryl ether sulphate (SLE$_3$S) here investigated.

The aim of this paper is to fill this gap in the knowledge, providing a systematic rheological characterisation
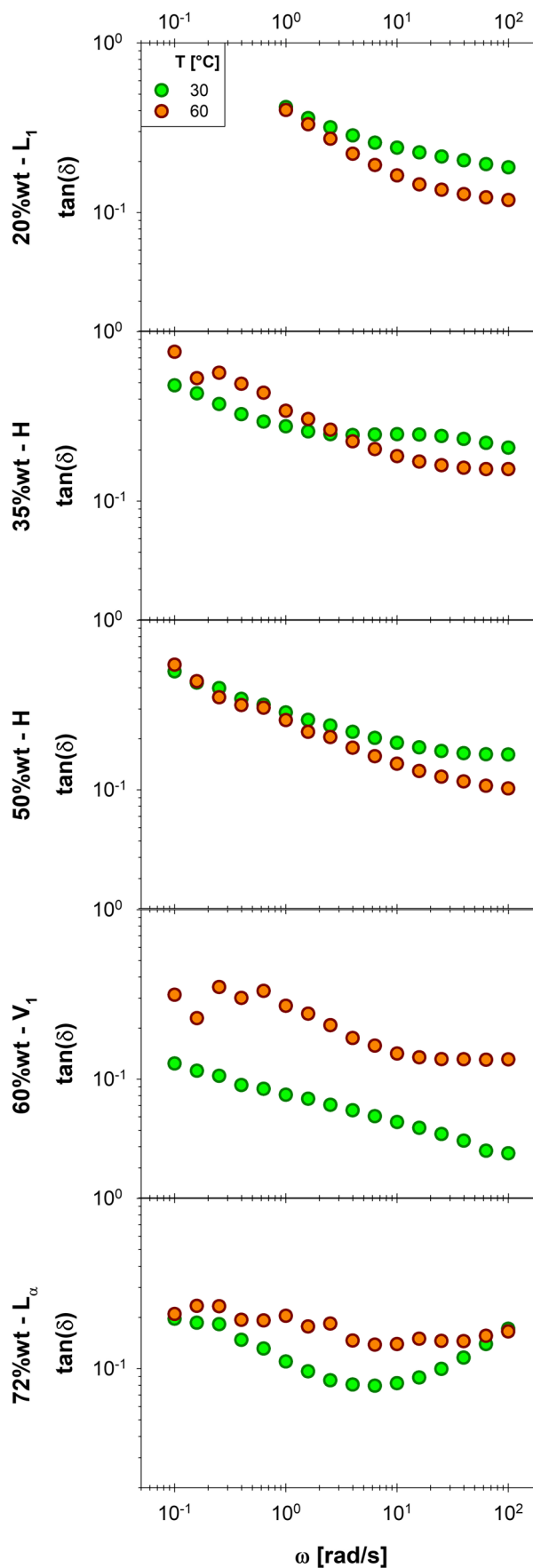
Fig. 7 Viscosity (**A**) and complex viscosity (**B**) against temperature, as function of SLE$_3$S concentration: 20%wt (triangle down), 35%wt (triangle up), 50%wt (circle), 60%wt (square) and 72%wt (diamond)
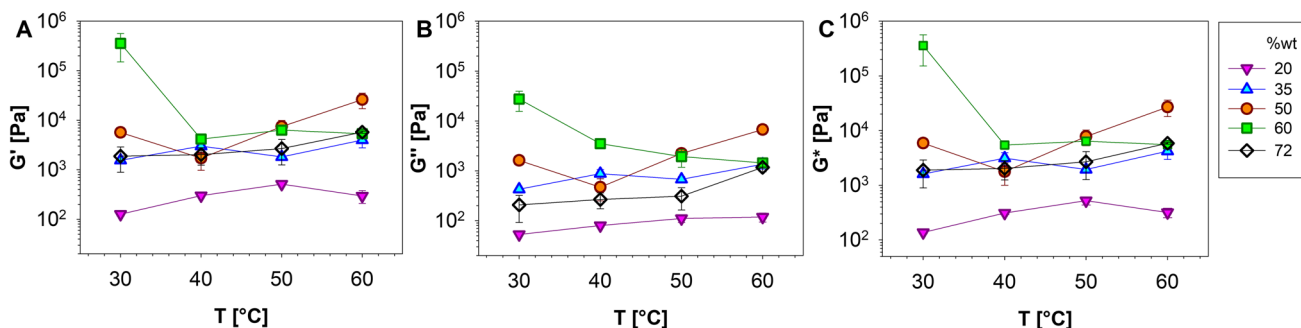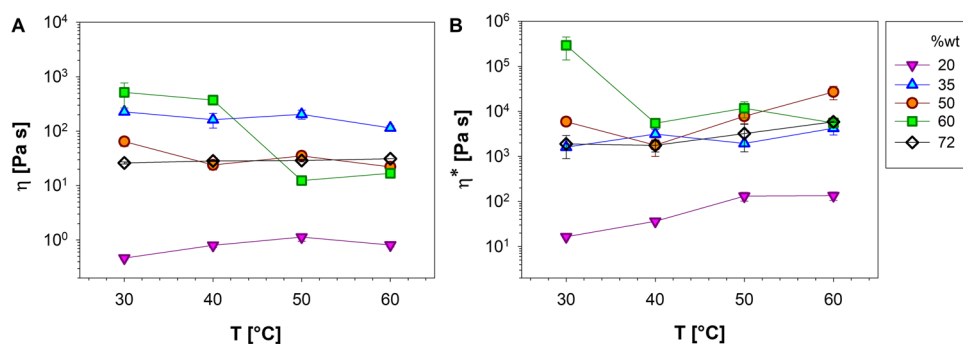

Fig. 8 Elastic (**A**), viscous (**B**) and complex modulus (**C**) against temperature, as function of SLE$_3$S concentration: 20%wt (triangle down), 35%wt (triangle up), 50%wt (circle), 60%wt (square) and 72%wt (diamond)

of SLE$_3$S, and demonstrate that rheology can be used in order to build such a phase diagram, being a suitable tool to recognise the phase transitions as function of concentration and temperature. In order to confirm the phase transition and to identify each phase, rheology is here supported by PLM, able to link optical anisotropy properties to different sample texture.

Sodium lauryl ether sulphate (SLE$_3$S) is investigated in a concentration (25–72%wt) and temperature (30–60 °C) range of technological relevance, collecting 20 measurement points. Each phase (micellar, hexagonal, cubic and lamellar, referred as L$_1$, H, V$_1$ and L$_\alpha$, respectively), at fixed temperature, shows non-monotonic changes of several orders of magnitude of distinct parameters: viscosity and complex viscosity, elastic, viscous and complex moduli. These results are obtained by analysing the system under steady and oscillatory shear flow. Increasing temperatures, H and L$_\alpha$ phases do not show significant rheological changes, in contrast to V$_1$ phase. In fact, rheological parameter of SLE$_3$S at 60%wt radically decreases by increasing temperature from 30 to 60 °C, confirming temperature-induced structural modifications.

The approach here proposed, focused on the range of concentration and temperature of industrial relevance, can be used as a simple and effective way to obtain a detailed phase map of a multicomponent mixtures

exhibiting complex phase behaviour, as was partially done in literature (Chopra et al. 2002; Ilyin et al. 2020; Pasquino et al. 2013). In fact, the approach here presented can be systematically applied to fine tune the characterisation, extending the number of temperature-concentration values, and to identify, with any needed precision, values of transition among phases. It is worth mentioning that surfactant systems can be affected by polydispersity due to the different preparation conditions, consequently, specific values of concentration and temperature related to phase transition could be affected. This aspect, increasing the range of frequencies investigated in order to identify the crossover point, could benefit from a more in-depth analysis (Escalante et al. 2000; Parker and Fieber 2013; Zou et al. 2015; Zou et al. 2019) in order to quantify parameter such as relaxation times, hydrodynamic correlation length, persistence length and average entanglement, to better describe each type of microstructure. Overall, the study of the phase diagram of aqueous surfactant solutions can benefit from the combined application of rheology and PLM, with other techniques, such as electron paramagnetic resonance spectroscopy and small-angle X-ray scattering, in order to characterise each microstructure.

Declarations

Conflict of interest The authors declare no competing interests.

References

Acharya DP, Kunieda H (2006) Wormlike micelles in mixed surfactant solutions. Adv Colloid Interface Sci 123:401–413

Baruah A, Pathak AK, Ojha K (2015) Phase behaviour and thermodynamic properties of lamellar liquid crystal developed for viscoelastic surfactant based fracturing fluid. Chem Eng Sci 131:146–154

Baruah A, Pathak AK, Ojha K (2016) Study on rheology and thermal stability of mixed (nonionic–anionic) surfactant based fracturing fluids. AIChE Journal 62:2177–2187

Capaccio A, Caserta S, Guido S, Rusciano G, Sasso A (2020) Dissolution of a surfactant-water lamellar phase investigated by combining time-lapse polarized light microscopy and confocal Raman spectroscopy. J Colloid Interface Sci 561:136–146

Cappelaere E, Cressely R, Makhloufi R, Decruppe JP (1994) Temperature and flow-induced viscosity transitions for CTAB surfactant solutions. Rheol Acta 33:431–437

Caserta S, Simeone M, Guido S (2004) Evolution of drop size distribution of polymer blends under shear flow by optical sectioning. Rheol Acta 43:491–501

Caserta S, Simeone M, Guido S (2006) A parameter investigation of shear-induced coalescence in semidilute PIB–PDMS polymer blends: effects of shear rate, shear stress volume fraction, and viscosity. Rheol Acta 45:505–512

Castaldo RI, Pasquino R, Villone MM, Caserta S, Gu C, Grizzuti N, Guido S, Maffettone PL, Guida V (2019) Dissolution of concentrated surfactant solutions: from microscopy imaging to rheological measurements through numerical simulations. Soft Matter 15:8352–8360

Chopra D, Kontopoulou M, Vlassopoulos D, Hatzikiriakos SG (2002) Effect of maleic anhydride content on the rheology and phase behavior of poly (styrene-co-maleic anhydride)/poly (methyl methacrylate) blends. Rheol Acta 41:10–24

Cserháti T, Forgács E, Oros G (2002) Biological activity and environmental impact of anionic surfactants. Environ Int 28:337–348

Davies TS, Ketner AM, Raghavan SR (2006) Self-assembly of surfactant vesicles that transform into viscoelastic wormlike micelles upon heating. J Am Chem Soc 128:6669–6675

Dehghan AA, Masihi M, Ayatollahi S (2015) Phase behavior and interfacial tension evaluation of a newly designed surfactant on heavy oil displacement efficiency; effects of salinity, wettability, and capillary pressure. Fluid Phase Equilibria 396:20–27

Drakontis CE, Amin S (2020) Biosurfactants: formulations, properties, and applications. Curr Opin Colloid Interface Sci 48:77–90

Escalante JI, Gradzielski M, Hoffmann H, Mortensen K (2000) Shear-induced transition of originally undisturbed lamellar phase to vesicle phase. Langmuir 16:8653–8663

Ferraro R, Ascione F, Dogra P, Cristini V, Guido S, Caserta S (2022) Diffusion-induced anisotropic cancer invasion: a novel experimental method based on tumour spheroids. AIChE Journal e17658

Fontell K (1990) Cubic phases in surfactant and surfactant-like lipid systems. Colloid Polym Sci 268:264–285

Garti N, Libster D, Aserin A (2012) Lipid polymorphism in lyotropic liquid crystals for triggered release of bioactives. Food Funct 3:700–713

Guo C, Wang J, Cao F, Lee RJ, Zhai G (2010) Lyotropic liquid crystal systems in drug delivery. Drug Discov Today 15:1032–1040

Hait SK, Moulik SP (2001) Determination of critical micelle concentration (CMC) of nonionic surfactants by donor-acceptor interaction with Iodine and correlation of CMC with hydrophile-lipophile balance and other parameters of the surfactants. J Surfactant Deterg 4:303–309

Hargreaves AE (2007) Chemical formulation: an overview of surfactant based chemical preparations used in everyday life

Ilyin SO, Makarova VV, Polyakova MY, Kulichikhin VG (2020) Phase state and rheology of polyisobutylene blends with silicone resin. Rheol Acta 59:375–386

Imae T, Kamiya R, Ikeda S (1985) Formation of spherical and rod-like micelles of cetyltrimethylammonium bromide in aqueous NaBr solutions. J Colloid Interface Sci 108:215–225

Jiang R, Huang Y-X, Zhao J-X, Huang C-C (2009) Aqueous two-phase system of an anionic gemini surfactant and a cationic conventional surfactant mixture. Fluid phase equilibria 277:114–120

Johnston MA, Swope WC, Jordan KE, Warren PB, Noro MG, Bray DJ, Anderson RL (2015) Toward a standard protocol for micelle simulation. J Phys Chem B 120:6337–6351

Kalur GC, Frounfelker BD, Cipriano BH, Norman AI, Raghavan SR (2005) Viscosity increase with temperature in cationic surfactant solutions due to the growth of wormlike micelles. Langmuir 21:10998–11004

Kekicheff P, Grabielle-Madelmont C, Ollivon M (1989) Phase diagram of sodium dodecyl sulfate-water system: 1. A calorimetric study. J Colloid Interface Sci 131:112–132

Kumaran V, Jariwala SK, Hussain S (2001) Rheology of a lamellar liquid crystalline phase using the lattice Boltzmann simulation technique. Chem Eng Sci 56:5663–5673

Lavergne A, Zhu Y, Pizzino A, Molinier V, Aubry J-M (2011) Synthesis and foaming properties of new anionic surfactants based on a renewable building block: sodium dodecyl isosorbide sulfates. J Colloid Interface Sci 360:645–653

Li H, Dang L, Yang S, Li J, Wei H (2016) The study of phase behavior and rheological properties of lyotropic liquid crystals in the LAS/AES/H2O system. Colloids Surf A Physicochem Eng Asp 495:221–228

Luo M, Jia Z, Sun H, Liao L, Wen Q (2012) Rheological behavior and microstructure of an anionic surfactant micelle solution with pyroelectric nanoparticle. Colloids Surf A Physicochem Eng Asp 395:267–275

Mahmood ME, Al-Koofee DAF (2013) Effect of temperature changes on critical micelle concentration for tween series surfactant. Global Journal of Science Frontier Research Chemistry 13:1–7

Ohlendorf D, Interthal W, Hoffmann H (1986) Surfactant systems for drag reduction: physico-chemical properties and rheological behaviour. Rheol Acta 25:468–486

Panmai S, Prud'homme RK, Peiffer DG (1999) Rheology of hydrophobically modified polymers with spherical and rod-like surfactant micelles. Colloids Surf A Physicochem Eng Asp 147:3–15

Panoukidou M, Wand CR, Del Regno A, Anderson RL, Carbone P (2019) Constructing the phase diagram of sodium laurylethoxysulfate using dissipative particle dynamics. J Colloid Interface Sci 557:34–44

Parker A, Fieber W (2013) Viscoelasticity of anionic wormlike micelles: effects of ionic strength and small hydrophobic molecules. Soft Matter 9:1203–1213

Pasquino R, Nicodemi F, Vanzanella V, Alfani R, Grizzuti N (2013) A rheological phase diagram of additives for cement formulations. Rheol Acta 52:395–401

Pommella A, Caserta S, Guida V, Guido S (2012) Shear-induced deformation of surfactant multilamellar vesicles. Phys Rev Lett 108:138301. https://doi.org/10.1103/PhysRevLett.108.138301

Poulos AS, Jones CS, Cabral JT (2017) Dissolution of anionic surfactant mesophases. Soft Matter 13:5332–5340

Rekvig L, Kranenburg M, Vreede J, Hafskjold B, Smit B (2003) Investigation of surfactant efficiency using dissipative particle dynamics. Langmuir 19:8195–8205

Richtering W (2001) Rheology and shear induced structures in surfactant solutions. Curr Opin Colloid Interface Sci 6:446–450

Skartlien R, Sollum E, Akselsen A, Meakin P (2012) Direct numerical simulation of surfactant-stabilized emulsions. Rheologica acta 51:649–673

Tomaiuolo G, Carciati A, Caserta S, Guido S (2016) Blood linear viscoelasticity by small amplitude oscillatory flow. Rheologica Acta 55:485–495

Trappe V, Weitz DA (2000) Scaling of the viscoelasticity of weakly attractive particles. Phys Rev Lett 85:449

Trickett K, Eastoe J (2008) Surfactant-based gels. Adv Colloid Interface Sci 144:66–74

Yang J (2002) Viscoelastic wormlike micelles and their applications. Curr Opin Colloid Interface Sci 7:276–281

Zhang Y, Han Y, Chu Z, He S, Zhang J, Feng Y (2013) Thermally induced structural transitions from fluids to hydrogels with pH-switchable anionic wormlike micelles. J Colloid Interface Sci 394:319–328

Zou W, Tan G, Jiang H, Vogtt K, Weaver M, Koenig P, Beaucage G, Larson RG (2019) From well-entangled to partially-entangled wormlike micelles. Soft Matter 15:642–655

Zou W, Tang X, Weaver M, Koenig P, Larson RG (2015) Determination of characteristic lengths and times for wormlike micelle solutions from rheology using a mesoscopic simulation method. J Rheol 59:903–934